Development 138, 2369-2378 (2011) doi:10.1242/dev.060160

Peter Pan functions independently of its role in ribosome biogenesis during early eye and craniofacial cartilage development in *Xenopus laevis*

Verena Bugner, Aleksandra Tecza, Susanne Gessert and Michael Kühl*

SUMMARY

The *Xenopus* oocyte possesses a large maternal store of ribosomes, thereby uncoupling early development from the de novo ribosome biosynthesis required for cell growth. Brix domain-containing proteins, such as Peter Pan (PPan), are essential for eukaryotic ribosome biogenesis. In this study, we demonstrate that PPan is expressed maternally as well as in the eye and cranial neural crest cells (NCCs) during early *Xenopus laevis* development. Depletion of PPan and interference with rRNA processing using antisense morpholino oligonucleotides resulted in eye and cranial cartilage malformations. Loss of PPan, but not interference with rRNA processing, led to an early downregulation of specific marker genes of the eye, including *Rx1* and *Pax6*, and of NCCs, such as *Twist*, *Slug* and *FoxD3*. We found that PPan protein is localized in the nucleoli and mitochondria and that loss of PPan results in increased apoptosis. These findings indicate a novel function of PPan that is independent of its role in ribosome biogenesis.

KEY WORDS: Peter Pan, Ssf1, Eye, Neural crest, Ribosome, Apoptosis, *Xenopus laevis*

INTRODUCTION

Cell growth, cell proliferation and differentiation are tightly regulated and highly interconnected during development. Early embryogenesis is characterized by a rapid cell cycle with a short G1 phase. This reduces the 'window of opportunity' for differentiation, which can only occur during G1 phase (Singh and Dalton, 2009). Before dividing, cells have to grow to ensure that the daughter cells are equal in size to the parental cells. Cell growth is mainly characterized by rRNA synthesis and ribosome biogenesis during the G1 phase. A rapid cell cycle can thus only be achieved in small cells (such as embryonic stem cells) or in embryos that can rely on large maternal ribosome stores, such as in *Xenopus laevis*.

Each *Xenopus* oocyte contains ~10^{12} ribosomes, which is sufficient for the requirements of ~10^6 cells at the end of embryogenesis (Pierandrei-Amaldi and Amaldi, 1994). Ribosome biogenesis occurs in a specialized subnuclear structure termed the nucleolus. In homozygous anucleolate mutants, no rRNA can be synthesized; however, embryos survive until the swimming tadpole stage, indicating that maternal ribosomes last until hatching (Brown, 1964). It is well documented in *Xenopus* embryos that the nucleoli reform during the gastrula stage. This event is accompanied by a weak resumption of rRNA precursor transcription (Busby and Reeder, 1982) and a slow recovery of ribosomal protein synthesis (Pierandrei-Amaldi and Amaldi, 1994; Verheggen et al., 1998). The synthesis of ribosomal proteins is significantly upregulated at stage 26, apparently when the number of maternal ribosomes drops below a certain threshold required to assure sufficient protein synthesis in some cells (Pierandrei-Amaldi and Amaldi, 1994). These data suggest that highly proliferative tissues require de novo synthesis of ribosomes earlier than other tissues during embryogenesis. The proto-oncogene *c-Myc* increases the efficiency of ribosome biogenesis by regulating the activity of all three RNA polymerases (I-III), thus enhancing the synthesis of rRNA and proteins essential for ribosome formation (Arabi et al., 2005; Grandori et al., 2005; Grewal et al., 2005).

The rRNA precursor undergoes highly complex processing that includes several specific endo- and exonucleolytic cleavages (reviewed by Henras et al., 2008). The precursor rRNA assembles with non-ribosomal proteins and small nucleolar ribonucleoprotein particles (snoRNPs) to form pre-ribosomal particles. Ssf1, which is one of these non-ribosomal proteins, is one of the five members of the Brix domain-containing protein family known in yeast, all of which are exclusively located in the nucleoli and essential for normal growth and viability owing to their function in rRNA processing (Bogengruber et al., 2003; Eisenhaber et al., 2001). Within the Brix domain, a σ^{70}-like motif can be identified. In prokaryotes, the σ^{70} subunit of RNA polymerase is involved in recognizing the transcription initiation site of target genes. In lower eukaryotes, proteins with a σ^{70}-like motif are able to bind to rRNA in vivo (Wehner and Baserga, 2002). Except one member, they contribute to the assembly of the large ribosomal subunit. Depletion of Ssf1 leads to premature cleavage of the rRNA precursor followed by the degradation of these aberrant cleavage products (Fatica et al., 2002), resulting in a loss of 5.8S rRNA. The homolog of Ssf1 in higher eukaryotes is Peter Pan (PPan). PPan was first identified in *Drosophila melanogaster* in a screen for larval growth defective mutants (Migeon et al., 1999). Similar to yeast Ssf1, PPan harbors a single globular Brix domain that includes a σ^{70}-like motif.

Owing to its large maternal ribosome stores, *X. laevis* is an ideal model organism with which to study PPan function during early vertebrate development, as this allows the analysis of PPan functions that are independent of ribosome biogenesis. We show that loss of PPan in anterior neural tissue results in morphological

Institute for Biochemistry and Molecular Biology, Ulm University, Albert-Einstein-Allee 11, D-89081 Ulm, Germany.

*Author for correspondence (michael.kuehl@uni-ulm.de)

Accepted 3 March 2011

defects in eye and craniofacial cartilage development. Similar effects were observed upon antisense morpholino oligonucleotide (MO)-based interference with rRNA processing. However, PPan downregulation, but not interference with rRNA processing, led to defects in eye field formation and neural crest (NC) induction. This study provides the first evidence for a bifunctional role of PPan during *Xenopus* development.

MATERIALS AND METHODS

Xenopus embryos and animal cap assay

X. laevis embryos were obtained, cultured and staged by standard methods (Nieuwkoop and Faber, 1975). For animal cap (AC) assays, the indicated MOs were injected bilaterally into the animal pole at the 2-cell stage. To neuralize ACs, 200 pg *noggin* RNA was co-injected. ACs were dissected at stage 9 and cultured to the equivalent of stage 13.

Cloning and mutagenesis

The PPan construct was obtained from RZPD (Deutsches Ressourcenzentrum für Genomforschung; clone IRBHp990E0270D, accession BC086267) and subcloned into pCS2+ (Rupp and Weintraub, 1991). From this construct, the Δ5′UTR PPan construct was amplified. PPanΔσ^{70} was generated from Δ5′UTR PPan by inverse PCR. The *c-Myc* ORF was isolated from stage 17 embryos. Primers correspond to *c-Myc-I* (accession X14806). All constructs were amplified using Pfu Ultra II DNA polymerase (Stratagene), cloned into pCS2+ and verified by sequencing. Primer sequences are given in Table S1 in the supplementary material.

Whole-mount in situ hybridization

For the preparation, hybridization and staining of embryos standard protocols were used (Hemmati-Brivanlou et al., 1990). Afterwards, embryos were bleached in 30% H_2O_2. For vibratome sections (25 μm) embryos were prepared as described (Gessert et al., 2007).

Antisense MOs and MO specificity tests

MOs were obtained from Gene Tools: PPan MO1, 5′-TCTTATC-TTTCCCCATGTTGCCAGA-3′; PPan MO2, 5′-CCACGTGGAAC-AGCAAAACCTCTTC-3′; and ITS2 MO, 5′-CGGGGGCGATGG-ACGTC*GGAGCGAC*-3′ [italics indicate the 3′ end of the 5.8S rRNA; the rest is complementary to the 5′ end of the internal transcribed spacer 2 (ITS2)]. c-Myc, Wnt4, p53 and Fz3 MOs were used as previously described (Bellmeyer et al., 2003; Cordenonsi et al., 2003; Deardorff et al., 2001; Saulnier et al., 2002). The standard Control MO (Gene Tools) was used. Unless indicated otherwise, the MOs were injected into one animal-dorsal blastomere of 8-cell stage embryos. Unless indicated otherwise, MO doses were: PPan MO1 and MO2, p53 MO, 5 ng; ITS2 MO and Wnt4 MO, 10 ng; c-Myc MO, 20 ng; Fz3 MO, 15 ng. Doses of Control MO were matched to the highest dose of the other MOs per experiment. For all experiments, *GFP* mRNA (500 pg) was co-injected as a tracer.

The specificity of PPan MO1 and MO2 was tested in vitro using a transcription/translation assay (TNT-Kit, Promega). For an in vivo test, the PPan MO1 and MO2 binding sites, as well as the mutated MO1 binding site (from Δ5′UTR PPan), were cloned in frame with and in front of the *GFP* ORF in pCS2+. The indicated RNA (0.5 ng) and MO (5 ng) were co-injected bilaterally into 2-cell stage embryos and GFP translation was monitored at stage 17/18. Reduction of endogenous PPan upon PPan MO injection was analyzed at stage 13 either by freon extraction and western blot or by immunostaining of dissociated AC cells (see below).

Immunoprecipitation, freon extraction and western blot

For immunoprecipitation, human embryonic kidney (HEK293) cells were harvested, resuspended in NOP buffer (150 mM NaCl, 10 mM Tris-HCl pH 7.8, 1 mM $MgCl_2$, 0.75 mM $CaCl_2$, 2% Nonidet P40) and homogenized by passing cells through a 20-gauge needle. All steps were carried out at 4°C. Lysate was rocked for 20 minutes and then centrifuged for 10 minutes at 16,000 ***g***. Extract (150 μl) was preincubated with 30 μl of protein A-sepharose beads (Sigma-Aldrich) for 20 minutes and then centrifuged for 3 minutes at 16,000 ***g***. The beads were retained as a negative control. The supernatant was incubated with NOP buffer including polyclonal rabbit anti-human PPan antibody (1:10; Proteintech Group) for 45 minutes at 4°C, followed by 15 minutes on ice. Protein A-sepharose beads (50 μl) were then added, incubated at 4°C for 30 minutes followed by centrifugation for 3 minutes at 16,000 ***g***. The pellet was washed with IP buffer (50 mM Tris-HCl pH 8.5, 0.5 M NaCl, 0.05% Nonidet P40, 0.02% NaN_3). SDS loading buffer was added and samples were eluted from beads prior to SDS-PAGE and western blot.

To detect endogenous *Xenopus* PPan, five embryos were homogenized in 50 μl lysis buffer (20 mM Tris pH 7.5, 150 mM NaCl, 1 mM EDTA, 1 mM EGTA, 1% Triton X-100, 1 mM PMSF). Upon freon extraction, 15 μg total protein per sample was used for SDS-PAGE and western blot. The nitrocellulose membrane was blocked in 2% BSA in TBST (150 mM NaCl, 25 mM Tris, 2 mM KCl, pH 7.4) for 30 minutes at room temperature and then incubated with anti-PPan primary antibody (1:500) and HRP-conjugated secondary antibody (Dianova) diluted 1:20,000 in 2% BSA in TBST for 2 hours each at room temperature. Monoclonal anti-mouse β-Tubulin I+II (Sigma-Aldrich) was used to provide a loading control.

Cryosection and immunohistochemistry

At stage 42, embryos were fixed overnight in 4% paraformaldehyde (PFA) at 4°C and equilibrated in 80% methanol/20% DMSO overnight at –20°C. Preparation of embryos for cryostat sections (10 μm) was performed as described (Fagotto et al., 1999). For immunofluorescence stainings, slides were washed in acetone and air dried. After washing with DEPC-treated water and PBT (0.1% Triton X-100 in PBS), sections were blocked in 10% goat serum in PBT for 1 hour. Incubation with anti-PPan antibody (1:200) was performed overnight at 4°C. Sections were rinsed in PBT, blocked in 2% BSA in PBT and incubated with Alexa Fluor 488 secondary antibody (1:500; Invitrogen) for 1 hour at room temperature. Nuclei were counterstained with DAPI. Coverslips were mounted with Mowiol 4-88 in glycerol (Calbiochem).

AC cells were cultured until stage 13, dissociated in CMFM (88 mM NaCl, 1 mM KCl, 2.4 mM $NaHCO_3$, 7.5 mM Tris pH 7.6, 1 mM EDTA) for 30 minutes by gentle pipetting and transferred onto Superfrost Ultra Plus slides (Thermo Scientific). Cells were dried and fixed in 4% PFA for 15 minutes. The staining procedure was the same as for cryosections. Additional antibodies used were: mouse monoclonal anti-β-catenin primary antibody (1:100; Santa Cruz Biotechnology) and Cy3-conjugated goat anti-mouse secondary antibody (1:800; Dianova).

HEK293 cells were grown on coverslips, fixed in 4% PFA, washed in PBS, permeabilized in PBT and washed again. Cells were blocked with 0.5% BSA in PBS and incubated with anti-PPan antibody (1:100) and monoclonal anti-UBF1 antibody (1:100; Sigma-Aldrich) for 1 hour at room temperature. Cells were extensively washed in PBS and incubated with Alexa Fluor 488 anti-rabbit (1:500) and Cy3-conjugated goat anti-mouse (1:800) secondary antibodies for 1 hour at room temperature. Coverslips were mounted on slides using IS Mounting Medium DAPI (Dianova). MitoTracker Red CMXRos fluorescent dye was used to stain mitochondria following the manufacturer's protocol (Invitrogen).

Semi-quantitative RT-PCR and quantitative real-time PCR

Total RNA was isolated from anterior explants at stage 23 using the RNeasy Micro Kit (Qiagen), or from neuralized ACs at stage 13 using the peqGOLD RNAPure Kit (PEQLAB), following the manufacturers' protocols. For cDNA synthesis, Superscript II RNaseH reverse transcriptase (Invitrogen) and random primers were used. For quantitative real-time PCR, the QuantiTect SYBR Green PCR Kit (Qiagen) was used. Primer sequences are given in Table S1 in the supplementary material.

TUNEL assay

TUNEL stainings were performed to label apoptotic cells in whole embryos (Hensey and Gautier, 1998). Embryos were injected with the indicated MOs and cultivated until stage 13 or 23. The TUNEL assay was carried out as described (Gessert et al., 2007). Embryos showing at least a 3-fold difference in the number of apoptotic cells on the injected side as compared with the uninjected side were considered to exhibit a phenotype.

Caspase assay

Xenopus embryos were injected bilaterally at the 2-cell stage or bilaterally animal-dorsal at the 8-cell stage as indicated. At stage 13, ten embryos were collected per assay, which was performed using the Caspase 3/7 Glo Assay (Promega) as described (Boorse et al., 2006; Siegel et al., 2009).

Cartilage staining

To analyze the structure of the craniofacial cartilage, embryos at stage 48 were fixed in MEMFA (0.1 M MOPS pH 7.4, 2 mM EGTA, 1 mM $MgSO_4$, 4% formaldehyde) for 2 hours at room temperature. Cartilage staining was performed as described (Bellmeyer et al., 2003) and then the cartilages were isolated.

Statistics

P-values were calculated by a nonparametric Mann-Whitney rank sum test.

RESULTS

PPan is expressed in neural tissue of *X. laevis*

A comparison of the *X. laevis* PPan protein sequence with that of homologs in other organisms revealed a high degree of similarity, especially in the Brix domain (94-41%) and the σ^{70}-like motif (100-70%) (see Fig. S1 in the supplementary material). As a prerequisite for functional studies, we analyzed the spatial and temporal expression pattern of PPan during early embryogenesis. Semi-quantitative RT-PCR demonstrated that *PPan* is expressed maternally and constantly during *Xenopus* development (data not shown). Whole-mount in situ hybridization revealed that tissue-specific expression of *PPan* starts at stage 12. Staining in the neural plate was apparent at stages 12, 15 and 18, with an enrichment in the anterior (Fig. 1A-C). At tailbud stage 23, strong expression of *PPan* was observed in the developing eye and the migrating cranial neural crest cells (NCCs) (Fig. 1D). At stages 28 to 36, an accumulation of *PPan* transcripts persisted in the eye, the forebrain and midbrain, the branchial arches, the pronephros, the hypaxial muscles and in the blood islands on the ventral side of the embryo (Fig. 1E-G). Sections at stage 36 demonstrated *PPan* expression in the ciliary marginal zone (CMZ), the lens and in the branchial arches (Fig. 1H,I). We furthermore investigated the expression of PPan protein using an antibody that recognizes human as well as *Xenopus* PPan (see Fig. S2 in the supplementary material), which confirmed PPan localization in the CMZ and lens on cryosections (Fig. 1J).

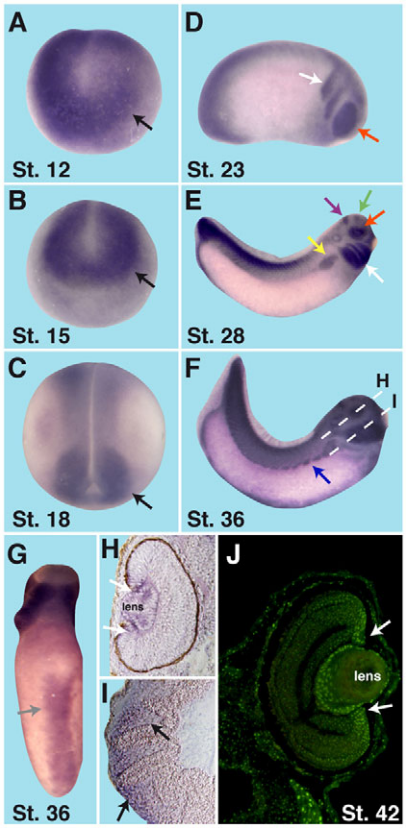

Fig. 1. The spatial expression pattern of *X. laevis* PPan. (**A-C**) *PPan* is expressed in the neural plate (arrows), as monitored from stage 12 to 18. (**D**) At stage 23, *PPan* transcripts accumulate in the eye (red arrow), the cranial neural crest cells (NCCs; white arrow), and in the posterior part of the embryo (left). (**E**) Arrows point to the different *PPan* expression domains at stage 28: eye (red), forebrain (green), midbrain (violet), branchial arches (white) and pronephros (yellow). (**F**,**G**) *PPan* is expressed in the hypaxial muscles (F, arrow) and the blood islands (G, arrow) at stage 36. (**H**) Transverse section (plane indicated in F) of the eye at stage 36 shows *PPan* expression in the ciliary marginal zone (CMZ; arrows) and in the lens. (**I**) Transverse section (plane indicated in F) at stage 36 indicates *PPan* expression in the branchial arches (arrows). (**J**) Transverse section of the eye shows PPan protein localized in the CMZ (arrows) and in the lens.

PPan functions in eye and cranial cartilage development

Since PPan is expressed in neural tissue, we next investigated the function of PPan during anterior neural development by performing gain- and loss-of-function studies. For knockdown approaches, we designed two antisense MOs directed against the translation initiation site of *PPan*. The specificity and efficiency of PPan MO1 and MO2 were confirmed in vitro and in vivo by several independent assays. An in vitro transcription/translation assay revealed that both PPan MOs, but not Control MO, were able to efficiently block the translation of PPan (see Fig. S3D in the supplementary material). For in vivo analysis, we cloned the PPan MO1 and MO2 binding sites (see Fig. S3A in the supplementary material) in frame with and in front of *GFP*. The RNA of these constructs was co-injected with the corresponding PPan MO or Control MO bilaterally into 2-cell stage embryos. GFP expression was examined at stage 17/18. Injection of PPan MO1 or MO2, but not Control MO, blocked GFP expression (see Fig. S3E in the supplementary material). Both assays showed that the Δ5′UTR PPan construct (see Fig. S3B in the supplementary material) is not targeted by PPan MO1 and thus could be used for rescue experiments. Furthermore, we tested the ability of PPan MO1 to reduce endogenous PPan levels by injecting 20 ng PPan MO1 into the animal pole. Immunostaining indicated a reduction of PPan protein (Fig. 2B), which was confirmed by western blot analyses (see Fig. S3C in the supplementary material). These data indicate that the PPan MOs specifically knock down PPan in *Xenopus* embryos.

To manipulate neural tissue we injected both MOs individually into one animal-dorsal blastomere of 8-cell stage embryos (Moody and Kline, 1990). *GFP* RNA was injected as a lineage tracer in all subsequent experiments to validate proper injection in anterior neural tissue and to identify the manipulated side of the embryo (see Fig. S4 in the supplementary material). Microinjection of PPan MO1 resulted in a severe eye phenotype in a dose-dependent manner, clearly visible at stage 40 (Fig. 2C). The retinal pigmented epithelium (RPE) was malformed, strongly reduced or completely absent upon PPan MO1

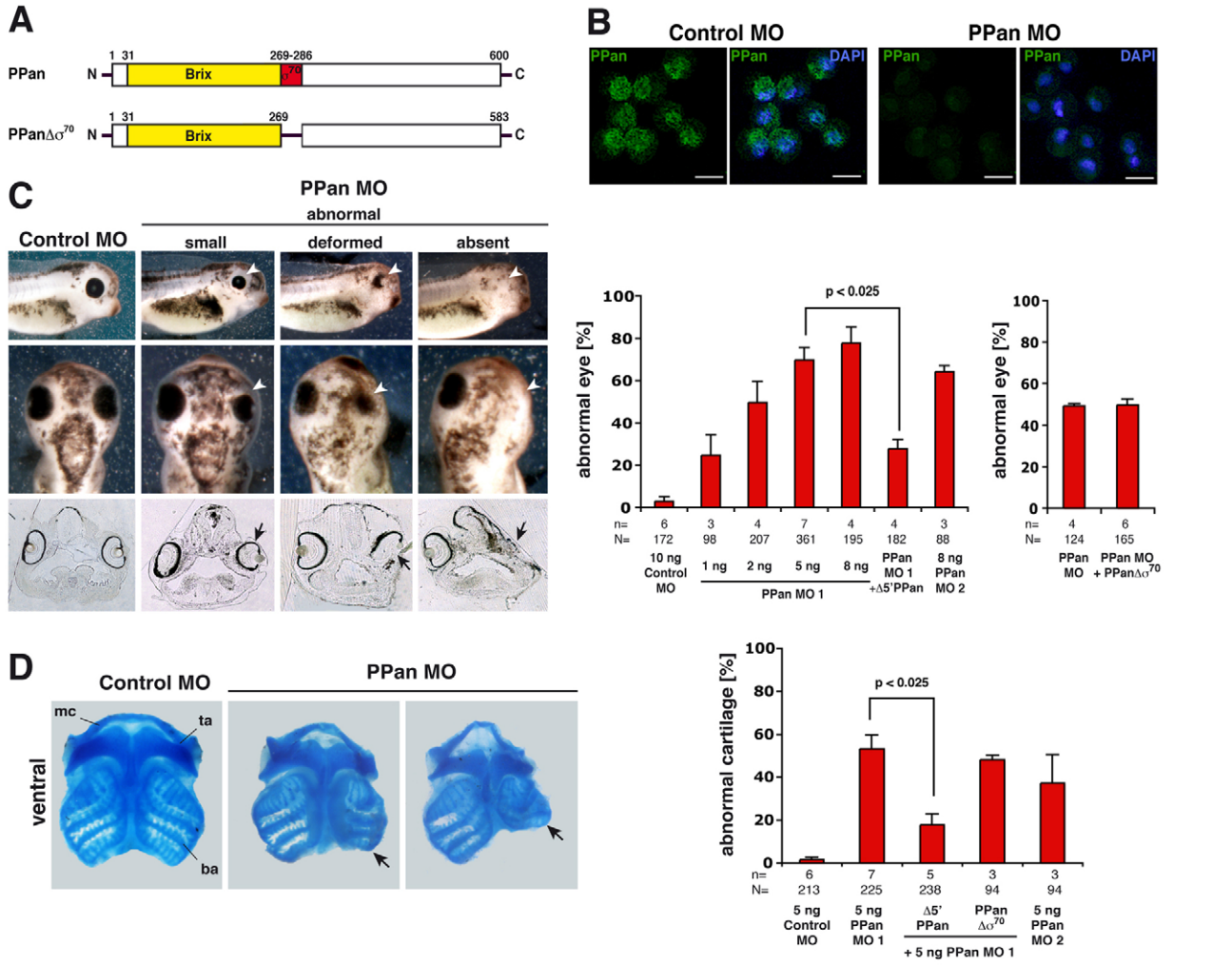

Fig. 2. Loss of PPan function strongly affects eye and craniofacial cartilage formation. (**A**) Schematic of *Xenopus* PPan protein illustrating the Brix domain (yellow) and σ^{70}-like motif (red). Beneath is illustrated the σ^{70} deletion construct PPan$\Delta\sigma^{70}$. (**B**) Endogenous PPan is strongly reduced in cells derived from PPan MO-injected *Xenopus* animal caps (ACs), as compared with Control MO-injected ACs. Scale bars: 20 μm. (**C**,**D**) PPan MO1 and MO2, but not Control MO, injection results in a severe eye (C) and cranial cartilage (D) phenotype on the injected side (arrowheads and arrows) in a dose-dependent manner. Co-injection of Δ5′UTR PPan RNA rescues PPan MO1-induced phenotypes, whereas PPan$\Delta\sigma^{70}$ does not. ba, branchial arches; mc, Meckel's cartilage; ta, tectum anterius. Quantitative evaluations are given to the right. *n*, number of independent experiments; *N*, total number of embryos examined. Error bars indicate s.e.m.

injection, as compared with Control MO-injected embryos. Histological sections at stage 42 further displayed defects in the lens and the multilayered retina. The same phenotype was observed after injection of PPan MO2. For all further experiments, we used 5 ng PPan MO1 (hereafter PPan MO). Co-injection of PPan MO and 2 ng Δ5′UTR PPan RNA significantly rescued the eye phenotype, indicating the specificity of the MO (Fig. 2C and see Fig. S5 in the supplementary material).

To determine whether the σ^{70}-like rRNA-binding domain is important for PPan function in *Xenopus* eye development, we generated a σ^{70} deletion construct (PPan$\Delta\sigma^{70}$) (Fig. 2A). Co-injection of PPan$\Delta\sigma^{70}$ RNA with PPan MO could not rescue PPan depletion (Fig. 2C). In addition, embryos injected unilaterally with PPan MO1 or MO2, but not Control MO, displayed severe defects in craniofacial cartilage development as shown by Alcian Blue staining at stage 48 (Fig. 2D). Similar to the eye phenotype, co-injection of Δ5′UTR PPan, but not PPan$\Delta\sigma^{70}$, RNA was able to revert the phenotype (Fig. 2D and see Fig. S5 in the supplementary material). In summary, our data indicate that PPan, and the σ^{70}-like motif in particular, is essential for eye as well as cranial cartilage development in *Xenopus*.

Interference with rRNA processing phenocopies PPan depletion

The best characterized function of PPan is in rRNA processing and thus ribosome biogenesis. Depletion of the PPan homolog Ssf1 in yeast leads to a reduced amount of mature 5.8S rRNA due to interference with rRNA processing (Fatica et al., 2002; Kaser et al., 2001). Thus, PPan MO injection should result in a reduction of 5.8S rRNA and interference with rRNA processing should lead to similar eye and cartilage malformations as noted above. To interfere with rRNA precursor processing we designed ITS2 MO, which targets the rRNA precursor at the junction between 5.8S rRNA and the internal transcribed spacer 2 (ITS2) sequence. Thus, this MO resembles the splicing MOs and should interfere with the cleavage of 5.8S rRNA (Fig. 3A). Furthermore, this region includes

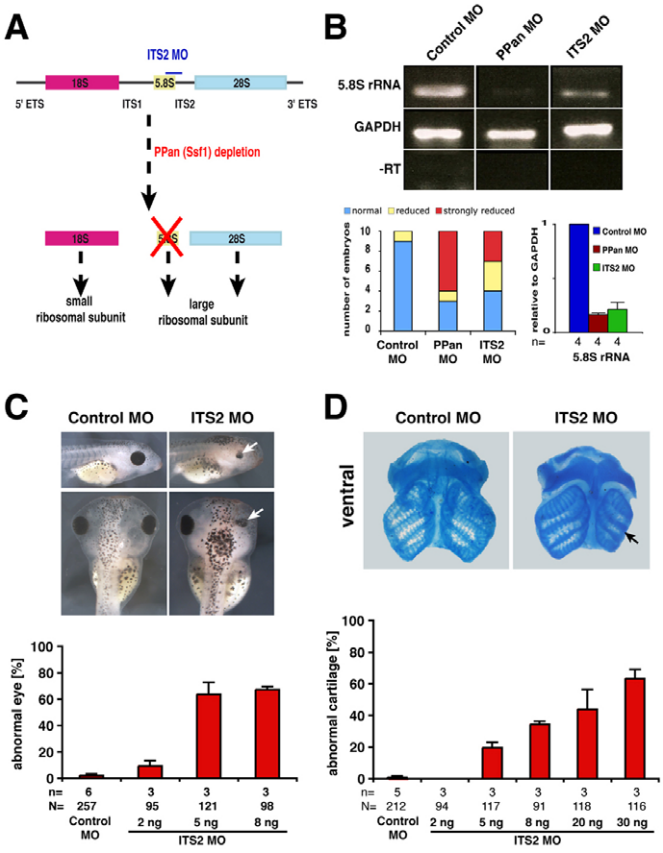

Fig. 3. Interference with ribosome biogenesis phenocopies PPan knockdown. (**A**) *Xenopus* 28S, 18S and 5.8S rRNAs are transcribed as a common rRNA precursor separated by the internal transcribed spacers 1 and 2 (ITS1 and ITS2). The binding site of ITS2 MO is indicated. ETS, external transcribed spacer. (**B**) Both PPan MO and ITS2 MO injection resulted in reduced 5.8S rRNA levels in anterior neural tissue at stage 23. Ten individual explants per MO were analyzed by RT-PCR. The agarose gel shows representative examples for reduced (ITS2 MO) and strongly reduced (PPan MO) signals. qRT-PCR analyses are also given (right). The data are presented as relative units normalized to Control MO-injected samples. (**C**,**D**) ITS2 MO injection into one animal-dorsal blastomere at the 8-cell stage results in severe eye (C) and craniofacial cartilage (D) defects in a dose-dependent manner (arrows). Quantitative evaluations are given beneath. *n*, number of independent experiments; *N*, total number of embryos examined. Error bars indicate s.e.m.

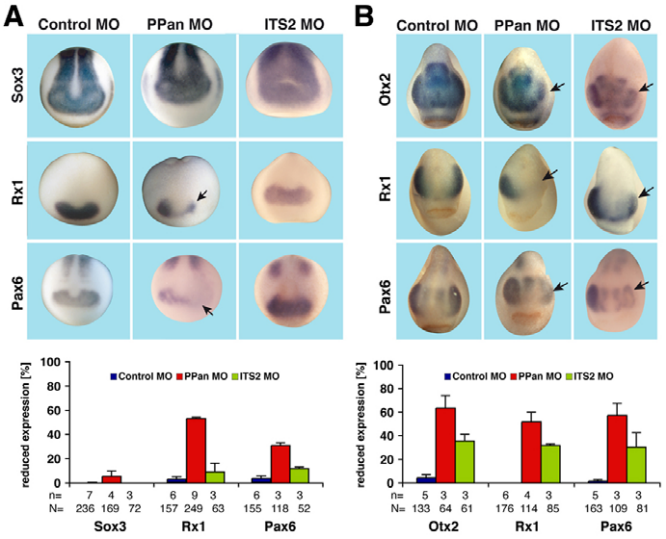

Fig. 4. PPan functions in early eye field induction. (**A**) Expression of *Sox3*, *Rx1* and *Pax6* was analyzed at stage 13. PPan-depleted *Xenopus* embryos exhibit reduced expression of *Rx1* and *Pax6* in the eye field (arrows). (**B**) At stage 23, expression of *Otx2*, *Rx1* and *Pax6* was strongly reduced upon PPan MO injection and slightly reduced upon ITS2 MO injection on the affected side (arrows). Quantitative evaluations are given beneath. *n*, number of independent experiments; *N*, total number of embryos examined. Error bars indicate s.e.m.

a conserved binding site for the U8 small nucleolar RNA, which has been shown to be involved in rRNA precursor processing (Michot et al., 1999). Injection of PPan MO or ITS2 MO resulted in a significant reduction of 5.8S rRNA in anterior neural tissue, as judged by semi-quantitative and quantitative RT-PCR at stage 23 (Fig. 3B). Note that in none of the cases was 5.8S rRNA completely absent, as maternal ribosomes were still present. If PPan function in neural development is due to its involvement in rRNA processing then interference with this process should phenocopy the effect of PPan depletion. Indeed, injection of ITS2 MO into one animal-dorsal blastomere of 8-cell stage embryos was accompanied by severe malformation of the eye and craniofacial cartilage in a dose-dependent manner (Fig. 3C,D). In summary, these data indicate that interference with ribosome biogenesis in neural tissue affects eye and cranial cartilage development in a similar manner to PPan depletion.

PPan depletion affects eye field and NC induction

If the PPan phenotype is exclusively due to interference with ribosome biogenesis, then depletion of PPan should not have any effect on early development because of the large maternal ribosome stores. We analyzed the expression of early pan-neural, brain and eye marker genes. Neither PPan nor Control MO injection interfered with the expression of the pan-neural marker *Sox3* (Fig. 4A), indicating that a loss of PPan does not affect neural induction in general. Surprisingly, inhibition of PPan resulted in a strong reduction of *Rx1* and a more modest inhibition of *Pax6* expression at stage 13, whereas Control MO-injected embryos were unaffected (Fig. 4A). At stage 23, expression of *Rx1*, *Pax6* and *Otx2* was strongly downregulated upon PPan depletion (Fig. 4B). In some cases, *Pax6* was also downregulated in the more posterior neural plate (see Fig. S6A in the supplementary material). None of the MOs inhibited the expression of the forebrain marker *Emx1* or the midbrain-hindbrain boundary marker *En2* (see Fig. S6B in the supplementary material).

Since the craniofacial cartilage is a derivative of the NC, we expanded our study by investigating the expression of NC marker genes upon PPan depletion. First, we examined NC induction. At stage 16/17, the expression of *Slug*, *FoxD3* and *Twist* was moderately reduced on the PPan MO-injected side (Fig. 5A). Next, we found that PPan MO injection led to defects in NCC migration as visualized by reduced *Slug*, *FoxD3* and *Twist* expression at stages 20 and 23 (Fig. 5B,C). Control MO injection interfered neither with NCC induction nor migration (Fig. 5).

By contrast, interfering with rRNA processing by ITS2 MO injection influenced neither early *Sox3*, *Rx1* and *Pax6* expression (Fig. 4A) nor *Slug*, *FoxD3* and *Twist* expression (Fig. 5A), which is consistent with the idea that newly synthesized ribosomes are not required prior to approximately stage 26 (Pierandrei-Amaldi and

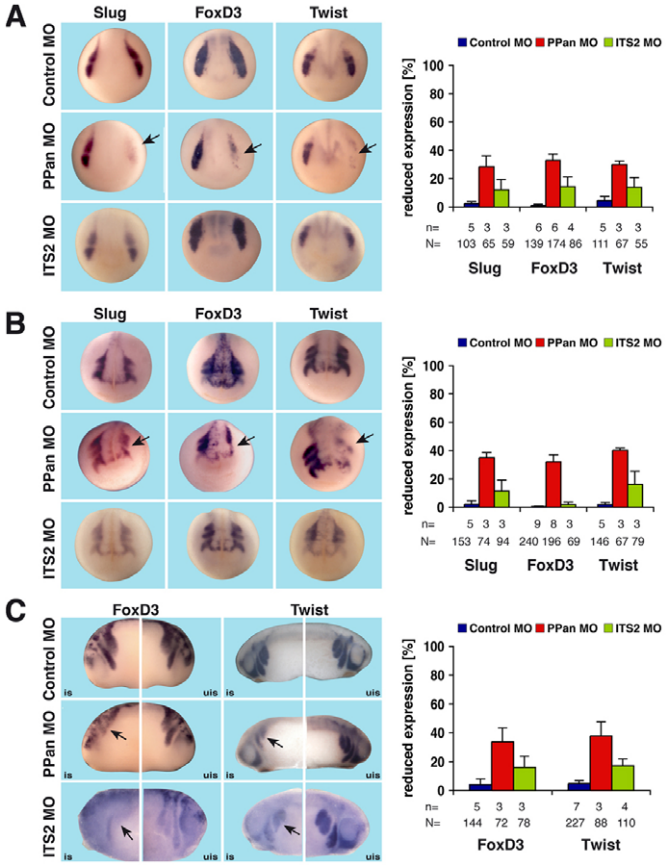

Fig. 5. PPan depletion results in defects in NC induction. (**A-C**) To study the behavior of NCCs upon PPan MO or ITS2 MO injection, *Slug*, *FoxD3* and *Twist* expression was analyzed. *Slug*, *FoxD3* and *Twist* expression at stages 16/17 (A) and 20 (B) as well as *FoxD3* and *Twist* expression at stage 23 (C) was reduced on the injected side upon PPan depletion, whereas ITS2 MO injection had little or no effect on NC specification and migration (arrows). Quantitative evaluations are given to the right. *n*, number of independent experiments; *N*, total number of embryos examined. Error bars indicate s.e.m.

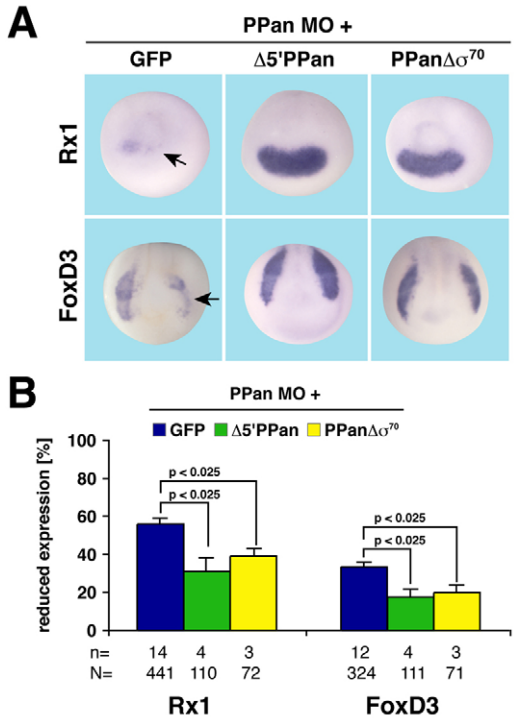

Fig. 6. Δ5′UTR PPan and PPanΔσ^{70} rescue defects in marker gene expression caused by PPan MO. (**A**) Co-injection of either 2 ng Δ5′UTR PPan or 2 ng PPanΔσ^{70} rescued the effect of 5 ng PPan MO on *Rx1* expression at stage 13 and *FoxD3* expression at stage 16 (arrows). (**B**) Quantification of the experiment in A. *n*, number of independent experiments; *N*, total number of embryos examined. Error bars indicate s.e.m.

Amaldi, 1994). Furthermore, both the Δ5′UTR PPan and PPanΔσ^{70} constructs significantly rescued the loss of marker gene expression to a similar extent (Fig. 6). These data indicate that loss of PPan function affects the induction of the eye field and NC independently of the de novo synthesis of ribosomes and thus point towards a novel function of PPan.

PPan is a potential target of Wnt signaling and acts upstream of Rx1, Pax6 and c-Myc

PPan and Wnt signaling are important for early eye and NC development. We therefore aimed to place PPan into a regulatory hierarchy with Wnt4 and the early eye and NC marker genes examined above. We also included *c-Myc* in these analyses as one of the earliest NC marker genes which is also expressed in the eye field (see Fig. S7A in the supplementary material) (Bellmeyer et al., 2003). Moreover, c-Myc regulates cell size by promoting rRNA and ribosomal protein synthesis, the cell cycle and differentiation. c-Myc MO injection led to eye and cranial cartilage defects in a dose-dependent manner, as observed upon PPan inhibition (see Fig. S7B,C in the supplementary material) (Bellmeyer et al., 2003).

PPan inhibition did not interfere with *Wnt4* expression at stage 13 (Fig. 7A). By contrast, depleting Wnt4 with a specific MO resulted in downregulation of *PPan* in embryos and neuralized animal caps (ACs) at the same stage, as monitored by semi-quantitative and quantitative RT-PCR (Fig. 7B and see Fig. S8 in the supplementary material). This also holds true at later stages (see Fig. S9 in the supplementary material). Taken together, these data place PPan downstream of Wnt4. In line with this, depletion of either Wnt4 or PPan resulted in downregulation of *Rx1*, *Pax6* and *c-Myc* at stage 13 (Fig. 7E,G). Overexpression of PPan did not result in enlarged or ectopic eye structures, indicating that PPan is required rather than instructive for eye formation (data not shown). Co-injection of 0.5 ng *PPan* RNA together with Wnt4 MO rescued expression of *c-Myc*, *Pax6* and *Rx1* (Fig. 7G). Depletion of c-Myc by a specific MO did not reduce *PPan* expression, confirming that PPan is upstream of c-Myc (Fig. 7B and see Fig. S8 in the supplementary material). c-Myc MO injection did not affect *Rx1* or *Pax6* expression (Fig. 7E,G), suggesting that c-Myc acts in parallel to or downstream of Rx1 and Pax6. Others have similarly placed Rx1 upstream of c-Myc during early eye development (Terada et al., 2006). In line with this, co-injection of *c-Myc* RNA (0.25-0.5 ng) could not revert the PPan MO-induced downregulation of *Rx1* and *Pax6* (Fig. 7G). Based on these findings we were able to generate a regulatory hierarchy of these factors in early eye development (Fig. 7C). During NC formation, both Wnt4 and PPan are required for the induction of *Slug*, *FoxD3* and *Twist* (Fig. 7F,H). Furthermore, co-injection of 2 ng *PPan* RNA reverted the Wnt4 MO-induced defects in *Slug*, *FoxD3* and *Twist* expression, giving

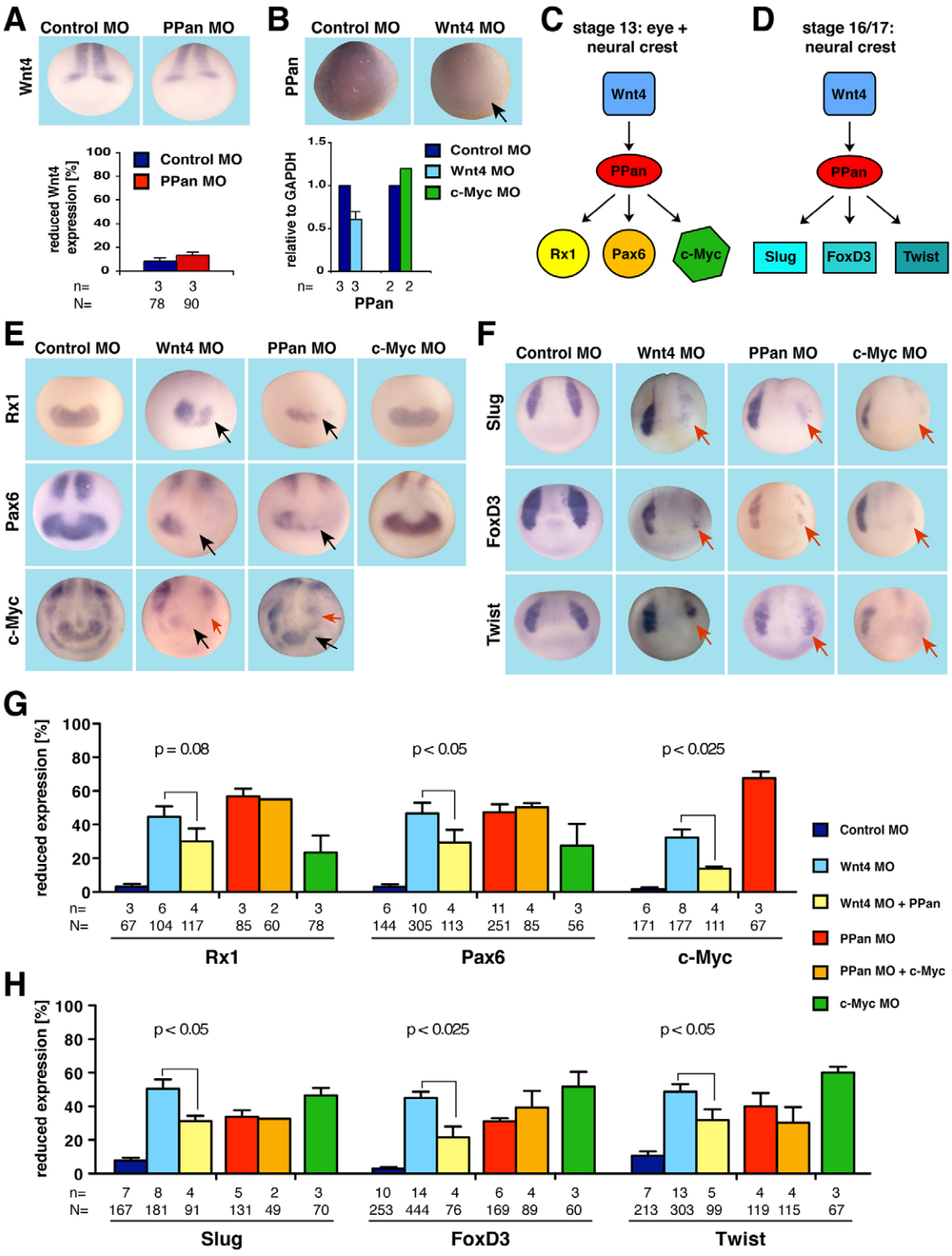

Fig. 7. PPan acts downstream of Wnt4. (**A**) PPan MO injection has no effect on *Wnt4* expression at stage 13. (**B**) Representative *Xenopus* embryos displaying reduced expression of *PPan* at stage 13 upon bilateral injection of 20 ng Wnt4 MO (animal-dorsal, 8-cell stage). For qRT-PCR analyses, embryos were injected with *noggin* RNA (200 pg) and Wnt4 MO (3 ng) or c-Myc MO (10 ng) bilaterally at the 2-cell stage. Noggin-induced neuralized ACs were dissected and cultured to the equivalent of stage 13. Data are presented as relative units normalized to Control MO-injected samples. (**C**) Hypothesis I. PPan acts downstream of Wnt4 and upstream of Rx1, Pax6 and c-Myc at stage 13 in the context of eye and NC development. (**D**) Hypothesis II. PPan acts between Wnt4 and NC-specific genes during NC induction. (**E**) Unilateral PPan MO as well as Wnt4 MO injection interfere with *Rx1*, *Pax6* and *c-Myc* expression on the injected side (black arrow, eye; red arrow, NC) at stage 13. By contrast, c-Myc MO has only a slight effect on *Rx1* and *Pax6* expression. (**F**) Wnt4, PPan and c-Myc depletion lead to a similar downregulation of the NC marker genes *Slug*, *FoxD3* and *Twist* at stage 16/17. (**G**,**H**) Quantification of the experiments in E (G) and F (H). Co-injection of *PPan* RNA rescues Wnt4 MO-induced reduction of all analyzed eye and NC marker genes. By contrast, co-injection of *c-Myc* RNA does not revert PPan MO-induced effects. *n*, number of independent experiments; *N*, total number of embryos examined. Error bars indicate s.e.m.

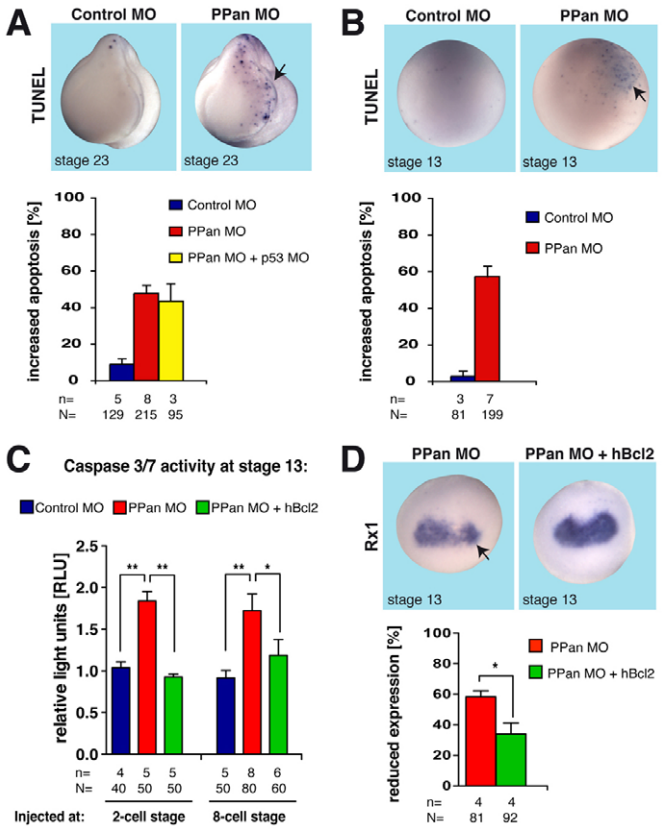

Fig. 8. PPan has a function in apoptosis. (**A**) Eight-cell stage *Xenopus* embryos were injected with PPan MO (5 ng) or Control MO (5 ng) into one animal-dorsal blastomere. TUNEL staining was used to label apoptotic cells. PPan depletion results in increased apoptosis on the manipulated side at stage 23 (arrow), which could not be rescued by co-injection of p53 MO (5 ng). Control MO-injected embryos were not affected. A quantitative evaluation is given beneath. (**B**) The increase in apoptosis can already be observed at stage 13. (**C**) Bilateral injection of 40 ng PPan MO at the 2-cell stage leads to increased activity of caspases 3 and 7. This effect can be reverted by co-injection of 4 ng human (h) *BCL2* RNA. The same effect was observed upon injection (bilateral, animal-dorsal) of 10 ng PPan MO and 2 ng human *BCL2* RNA at the 8-cell stage. Values represent relative light units (RLU) normalized to one Control MO-injected sample per series of experiments. (**D**) Co-injection of 1 ng human *BCL2* RNA into one animal-dorsal blastomere at the 8-cell stage rescued the PPan MO-induced reduction of *Rx1* expression (arrow). **, $P<0.01$; *, $P<0.05$. *n*, number of independent experiments; *N*, total number of embryos examined. Error bars indicate s.e.m.

rise to a similar hierarchy (Fig. 7D,H). We also found c-Myc to be upstream of Slug, FoxD3 and Twist (Fig. 7F,H), as shown previously by others (Bellmeyer et al., 2003; Schneider et al., 2010). Co-injection of *c-Myc* RNA (0.25-0.5 ng) together with PPan MO did not rescue the effects of PPan depletion on NC marker gene expression (Fig. 7H).

These findings reveal that PPan, among other proteins, partially mediates Wnt4 function in eye and NC development. The fact that c-Myc is unable to rescue the effects of PPan depletion on NC marker gene expression indicates that PPan action is required at several time points during NC development rather than just at the earliest time of induction. This might also be a first hint that PPan may be essential for maintaining signals towards NC development rather than being involved in NC induction.

PPan has a function in apoptosis

We further analyzed the effect of PPan on cell proliferation and apoptosis. At stage 23, unilateral PPan-depleted embryos showed increased apoptosis compared with Control MO-injected embryos (Fig. 8A). Apoptosis can be triggered by free ribosomal proteins that bind to and inhibit Mdm2, an E3 ubiquitin ligase for p53 (Dai et al., 2004). Interestingly, the observed increase in apoptosis could not be restored by co-injection of p53 MO, suggesting a more direct effect of PPan in apoptosis regulation. We also observed higher levels of apoptosis at stage 13 (Fig. 8B), whereas cell proliferation was not altered upon PPan depletion (data not shown). The observed apoptosis was accompanied by increased activity of the effector caspases 3 and 7 (Fig. 8C). The enhanced activity of the caspases was downregulated by co-injection of human *BCL2* RNA (Fig. 8C). These data indicate that PPan might have a direct anti-apoptotic function, suggesting that the observed phenotype could be due to increased apoptosis. Interestingly, co-injection of *BCL2* partially rescued Rx1 reduction upon PPan MO injection at stage 13 (Fig. 8D), indicating that the eye phenotype is indeed at least partially due to increased apoptosis.

PPan is localized to nucleoli and mitochondria

Our findings argue for a role of PPan that is independent of its function in ribosome biogenesis. We therefore analyzed the cellular localization of PPAN in HEK293 cells, as a heterologous cell system. Antibody stainings detected PPAN in the nucleoli of HEK293 cells. Nucleolar localization was confirmed by staining for upstream binding factor 1 (UBF1; also known as UBTF), which is required for rRNA synthesis (Fig. 9A). In addition, we detected endogenous PPAN within the cytoplasm in a punctate pattern (Fig. 9A and see Fig. S10A in the supplementary material). In neuralized *Xenopus* ACs, endogenous PPan was detected in the nucleoli as well as in the cytoplasm (Fig. 9C). Counterstaining AC cells with an anti-β-catenin antibody indicated that PPan is not localized at the cell membrane (Fig. 9D). Owing to its potential role in apoptosis regulation we counterstained the mitochondria using Mitotracker Red in HEK293 cells and found that PPAN is localized to this specific cell compartment (Fig. 9B and see Fig. S10B in the supplementary material). Unfortunately, we were unable to detect mitochondria-specific Mitotracker Red signal in dissociated AC cells because of the high autofluorescence of the yolk, a feature that has also been described by others (Inui and Asashima, 2004).

Taken together, our functional data and localization studies are clearly in agreement in indicating a novel function of PPan during cellular differentiation and in the regulation of apoptosis that is independent of its role in ribosome biogenesis.

DISCUSSION

Our observations have implications with respect to two issues: first, the requirement of de novo ribosome biogenesis during *Xenopus* development; and second, the identification of a novel function of the rRNA processing protein PPan during early development.

Requirement of ribosome biogenesis during *X. laevis* development

A major characteristic of early *Xenopus* embryogenesis is the maternal supply of mRNA and proteins, including substantial amounts of ribosomes, which allows for a rapid cell cycle. Earlier studies indicated that the formation of new ribosomes in *Xenopus* starts around stage 26 and that maternal ribosomes are able to cover the demands of the embryo until the swimming tadpole stage (Pierandrei-Amaldi and Amaldi, 1994). We show that interference

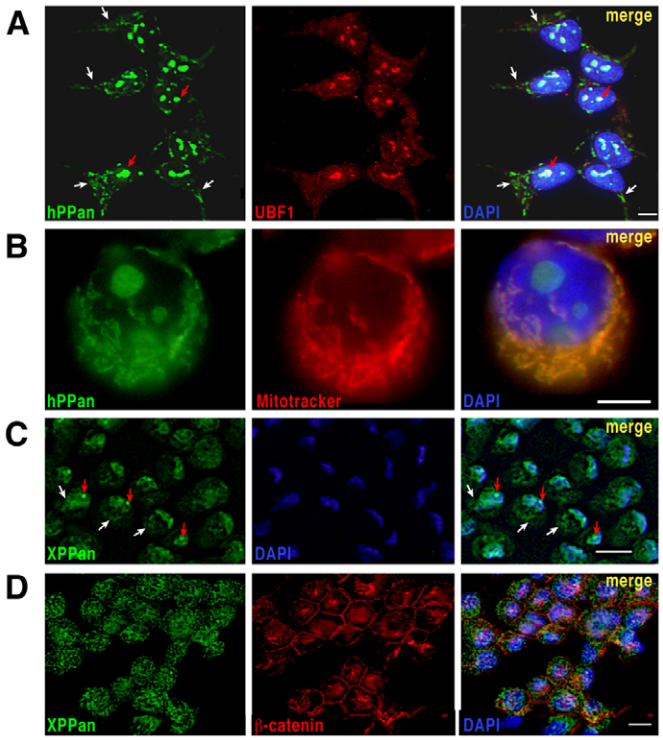

Fig. 9. Cellular localization of PPan. (**A**) Immunofluorescence staining of human PPAN (hPPan) and UBF1 in HEK293 cells by use of specific antibodies. The overlay shows the colocalization (red arrows) of PPAN (green) and UBF1 (red). White arrows indicate extranuclear PPAN. Nuclei are visualized by DAPI staining (blue). (**B**) PPAN is located in the mitochondria of HEK293 cells as shown by counterstaining with MitoTracker Red CMXRos. (**C**) Neuralized AC cells equivalent stage 13 were dissociated and stained for PPan (green). *Xenopus* (X) PPan is localized to the nucleoli (red arrows) and in the cytoplasm (white arrows) of neural cells. (**D**) Immunofluorescence staining in attached cells from untreated ACs revealed that *Xenopus* PPan (green) can be found in the cytoplasm but not at the cell membrane, which is labeled by β-catenin staining (red). Scale bars: 10 μm in A,B; 20 μm in C,D.

with mature rRNA formation by ITS2 MO injection results in eye and cranial cartilage defects. Interestingly, the anucleolate mutant also suffers from microcephaly, small eyes and reduced numbers of melanocytes [see figure 1 in the original paper describing the anucleolate mutant (Brown, 1964)]. Most likely, these data indicate that different cell types in the developing embryo require de novo generation of ribosomes at different time points. The eye and the developing NC are highly proliferative and are therefore among the first tissues that might suffer from insufficient maternal ribosome supply. A more in-depth analysis of the anucleolate mutant on a molecular level might therefore prove interesting.

There is good evidence to suggest that PPan is involved in the formation of ribosomes during later development. PPan belongs to the highly conserved Brix domain-containing protein family. Extensive studies in yeast revealed that the Brix domain has a function in biogenesis of the large ribosomal subunit (Bogengruber et al., 2003; Eisenhaber et al., 2001; Fatica et al., 2002) and that the associated σ^{70}-like motif is an rRNA-binding domain (Wehner and Baserga, 2002). Consistent with a potential function of PPan in ribosome biogenesis, we show that *Xenopus* PPan, similar to its homolog Ssf1 in yeast, is located in the nucleoli, where ribosome biogenesis mainly takes place (Scheer and Hock, 1999). In addition, we demonstrate that depletion of PPan results in reduced 5.8S rRNA levels later in development. It is noteworthy that PPan is especially expressed in the CMZ, a highly proliferative neuroepithelium within the eye that contains undifferentiated retinal progenitor cells (Perron et al., 1998). In amphibians the CMZ is responsible for the growth of the retina throughout adult life. This is in line with the argument that highly proliferative cells require a sufficient number of ribosomes.

Consistently, knockdown of PPan resulted in severe eye and craniofacial cartilage abnormalities. The eye phenotype includes smaller, deformed and completely absent eyes on the injected side. Interestingly, PPan$\Delta\sigma^{70}$ failed to rescue the PPan MO-induced phenotype, demonstrating the important role of the rRNA-binding domain. These results support the idea that PPan function in ribosome biogenesis is important for eye and craniofacial cartilage development. The confirmation of this hypothesis is, however, hampered by the earlier functions of PPan during eye and NC development (see below), which are likely to be independent of ribosome biogenesis.

PPan is required for early eye and NC differentiation

A more in-depth analysis of the molecular basis of the observed phenotypes indicated that PPan MO injection led to defects in eye field and NC induction. Additionally, we observed a disturbance in NCC migration upon PPan MO injection at later stages, in which the cells resided at the dorsal neural tube. These phenotypes are clearly not caused by dysregulation in rRNA precursor processing, as supported by the following findings: (1) injection of ITS2 MO results in a downregulation of 5.8S rRNA but did not result in embryonic phenotypes at stages 13 or 16/17; and (2) the PPan$\Delta\sigma^{70}$ mutant was able to rescue the early loss of marker genes.

By diverse loss-of-function experiments we aimed to place PPan within a network of regulatory interactions. The observation that *PPan* expression is dependent on Wnt4 at stage 13 (Fig. 7B) and on Wnt4 and Fz3 function at stage 23 (see Fig. S9 in the supplementary material) suggests that PPan might be a potential target of Wnt signaling on a transcriptional level. Furthermore, both Wnt4 and PPan are required for induction of early eye- and NC-specific marker genes. PPan was able to rescue the Wnt4 MO phenotype but was unable to generate ectopic eye structures upon overexpression. By contrast, it has been shown that Rx1 (Chuang and Raymond, 2002) and Wnt4 (Maurus et al., 2005) are sufficient to induce ectopic eye tissue in the nervous system of vertebrates. We therefore argue that PPan is required for Wnt4 function on a protein level rather than being an instructive component of the early eye and NC specification network. Further investigations are needed to determine whether PPan is required for the induction or maintenance of these genes.

Toward a molecular analysis of PPan function

We were able to demonstrate that PPan has a function in cell apoptosis but not proliferation as early as stage 13, when eye field and NC induction occur. Knockdown of PPan led to increased apoptosis in anterior neural tissue (Fig. 8). This effect was not blocked by simultaneous injection of a p53 MO, indicating that the apoptosis was not a non-specific toxic side effect of the injected MO (Robu et al., 2007) or due to free ribosomal proteins (Dai et al., 2004). This indicates that PPan might have direct anti-apoptotic functions early during development. In line with this, we observed that apoptosis could be rescued by co-injection of *BCL2* RNA and

that PPan is localized to the mitochondria. Also, the eye phenotype was partially reverted by *BCL2*, indicating that the phenotype is at least partially due to the increased apoptosis. Further efforts are required to identify how mitochondrial PPan acts in an anti-apoptotic manner.

In summary, PPan appears to link important processes during early development, including differentiation, proliferation and apoptosis. Future work will need to unravel the signaling pathways in which PPan is involved in order to uncover the molecular mechanisms that underlie PPan function. Identifying protein-protein interaction partners of PPan will be an important step in this direction.

Acknowledgements
We thank Doris Wedlich and Thomas Hollemann for helpful suggestions; Doreen Siegel and Tata Purushothama Rao for discussion; and Walter Knöchel, Tomas Pieler, Thomas Hollemann, Richard Harland, Michael Sargent and Doris Wedlich for providing plasmids. This project was supported by the DFG (SFB 497, TpA6). Verena Bugner and Aleksandra Tecza are members of the International Graduate School in Molecular Medicine Ulm (GSC270).

Competing interests statement
The authors declare no competing financial interests.

Supplementary material
Supplementary material for this article is available at
http://dev.biologists.org/lookup/suppl/doi:10.1242/dev.060160/-/DC1

References
Arabi, A., Wu, S., Ridderstrale, K., Bierhoff, H., Shiue, C., Fatyol, K., Fahlen, S., Hydbring, P., Soderberg, O., Grummt, I. et al. (2005). c-Myc associates with ribosomal DNA and activates RNA polymerase I transcription. *Nat. Cell Biol.* **7**, 303-310.
Bellmeyer, A., Krase, J., Lindgren, J. and LaBonne, C. (2003). The protooncogene c-myc is an essential regulator of neural crest formation in Xenopus. *Dev. Cell* **4**, 827-839.
Bogengruber, E., Briza, P., Doppler, E., Wimmer, H., Koller, L., Fasiolo, F., Senger, B., Hegemann, J. H. and Breitenbach, M. (2003). Functional analysis in yeast of the Brix protein superfamily involved in the biogenesis of ribosomes. *FEMS Yeast Res.* **3**, 35-43.
Boorse, G. C., Kholdani, C. A., Seasholtz, A. F. and Denver, R. J. (2006). Corticotropin-releasing factor is cytoprotective in Xenopus tadpole tail: coordination of ligand, receptor, and binding protein in tail muscle cell survival. *Endocrinology* **147**, 1498-1507.
Brown, D. D. (1964). RNA synthesis during amphibian development. *J. Exp. Zool.* **157**, 101-117.
Busby, S. J. and Reeder, R. H. (1982). Fate of amplified nucleoli in Xenopus laevis embryos. *Dev. Biol.* **91**, 458-467.
Chuang, J. C. and Raymond, P. A. (2002). Embryonic origin of the eyes in teleost fish. *BioEssays* **24**, 519-529.
Cordenonsi, M., Dupont, S., Maretto, S., Insinga, A., Imbriano, C. and Piccolo, S. (2003). Links between tumor suppressors: p53 is required for TGF-beta gene responses by cooperating with Smads. *Cell* **113**, 301-314.
Dai, M. S., Zeng, S. X., Jin, Y., Sun, X. X., David, L. and Lu, H. (2004). Ribosomal protein L23 activates p53 by inhibiting MDM2 function in response to ribosomal perturbation but not to translation inhibition. *Mol. Cell. Biol.* **24**, 7654-7668.
Deardorff, M. A., Tan, C., Saint-Jeannet, J. P. and Klein, P. S. (2001). A role for frizzled 3 in neural crest development. *Development* **128**, 3655-3663.
Eisenhaber, F., Wechselberger, C. and Kreil, G. (2001). The Brix domain protein family – a key to the ribosomal biogenesis pathway? *Trends Biochem. Sci.* **26**, 345-347.
Fagotto, F., Jho, E., Zeng, L., Kurth, T., Joos, T., Kaufmann, C. and Costantini, F. (1999). Domains of axin involved in protein-protein interactions, Wnt pathway inhibition, and intracellular localization. *J. Cell Biol.* **145**, 741-756.
Fatica, A., Cronshaw, A. D., Dlakic, M. and Tollervey, D. (2002). Ssf1p prevents premature processing of an early pre-60S ribosomal particle. *Mol. Cell* **9**, 341-351.
Gessert, S., Maurus, D., Rossner, A. and Kuhl, M. (2007). Pescadillo is required for Xenopus laevis eye development and neural crest migration. *Dev. Biol.* **310**, 99-112.
Grandori, C., Gomez-Roman, N., Felton-Edkins, Z. A., Ngouenet, C., Galloway, D. A., Eisenman, R. N. and White, R. J. (2005). c-Myc binds to human ribosomal DNA and stimulates transcription of rRNA genes by RNA polymerase I. *Nat. Cell Biol.* **7**, 311-318.
Grewal, S. S., Li, L., Orian, A., Eisenman, R. N. and Edgar, B. A. (2005). Myc-dependent regulation of ribosomal RNA synthesis during Drosophila development. *Nat. Cell Biol.* **7**, 295-302.
Hemmati-Brivanlou, A., Frank, D., Bolce, M. E., Brown, B. D., Sive, H. L. and Harland, R. M. (1990). Localization of specific mRNAs in Xenopus embryos by whole-mount in situ hybridization. *Development* **110**, 325-330.
Henras, A. K., Soudet, J., Gerus, M., Lebaron, S., Caizergues-Ferrer, M., Mougin, A. and Henry, Y. (2008). The post-transcriptional steps of eukaryotic ribosome biogenesis. *Cell. Mol. Life Sci.* **65**, 2334-2359.
Hensey, C. and Gautier, J. (1998). Programmed cell death during Xenopus development: a spatio-temporal analysis. *Dev. Biol.* **203**, 36-48.
Inui, M. and Asashima, M. (2004). Identification and characterization of Xenopus OMP25. *Dev. Growth Differ.* **46**, 405-412.
Kaser, A., Bogengruber, E., Hallegger, M., Doppler, E., Lepperdinger, G., Jantsch, M., Breitenbach, M. and Kreil, G. (2001). Brix from Xenopus laevis and brx1p from yeast define a new family of proteins involved in the biogenesis of large ribosomal subunits. *Biol. Chem.* **382**, 1637-1647.
Maurus, D., Heligon, C., Burger-Schwarzler, A., Brandli, A. W. and Kuhl, M. (2005). Noncanonical Wnt-4 signaling and EAF2 are required for eye development in Xenopus laevis. *EMBO J.* **24**, 1181-1191.
Michot, B., Joseph, N., Mazan, S. and Bachellerie, J. P. (1999). Evolutionarily conserved structural features in the ITS2 of mammalian pre-rRNAs and potential interactions with the snoRNA U8 detected by comparative analysis of new mouse sequences. *Nucleic Acids Res.* **27**, 2271-2282.
Migeon, J. C., Garfinkel, M. S. and Edgar, B. A. (1999). Cloning and characterization of peter pan, a novel Drosophila gene required for larval growth. *Mol. Biol. Cell* **10**, 1733-1744.
Moody, S. A. and Kline, M. J. (1990). Segregation of fate during cleavage of frog (Xenopus laevis) blastomeres. *Anat. Embryol. (Berl.)* **182**, 347-362.
Nieuwkoop, P. and Faber, J. (1975). External and internal stage criteria in the development of Xenopus laevis. Elsevier: Amsterdam.
Perron, M., Kanekar, S., Vetter, M. L. and Harris, W. A. (1998). The genetic sequence of retinal development in the ciliary margin of the Xenopus eye. *Dev. Biol.* **199**, 185-200.
Pierandrei-Amaldi, P. and Amaldi, F. (1994). Aspects of regulation of ribosomal protein synthesis in Xenopus laevis. *Genetica* **94**, 181-193.
Robu, M. E., Larson, J. D., Nasevicius, A., Beiraghi, S., Brenner, C., Farber, S. A. and Ekker, S. C. (2007). p53 activation by knockdown technologies. *PLoS Genet.* **3**, e78.
Rupp, R. A. and Weintraub, H. (1991). Ubiquitous MyoD transcription at the midblastula transition precedes induction-dependent MyoD expression in presumptive mesoderm of X. laevis. *Cell* **65**, 927-937.
Saulnier, D. M., Ghanbari, H. and Brandli, A. W. (2002). Essential function of Wnt-4 for tubulogenesis in the Xenopus pronephric kidney. *Dev. Biol.* **248**, 13-28.
Scheer, U. and Hock, R. (1999). Structure and function of the nucleolus. *Curr. Opin. Cell Biol.* **11**, 385-390.
Schneider, M., Schambony, A. and Wedlich, D. (2010). Prohibitin1 acts as a neural crest specifier in Xenopus development by repressing the transcription factor E2F1. *Development* **137**, 4073-4081.
Siegel, D., Schuff, M., Oswald, F., Cao, Y. and Knochel, W. (2009). Functional dissection of XDppa2/4 structural domains in Xenopus development. *Mech. Dev.* **126**, 974-989.
Singh, A. M. and Dalton, S. (2009). The cell cycle and Myc intersect with mechanisms that regulate pluripotency and reprogramming. *Cell Stem Cell* **5**, 141-149.
Terada, K., Kitayama, A., Kanamoto, T., Ueno, N. and Furukawa, T. (2006). Nucleosome regulator Xhmgb3 is required for cell proliferation of the eye and brain as a downstream target of Xenopus rax/Rx1. *Dev. Biol.* **291**, 398-412.
Verheggen, C., Le Panse, S., Almouzni, G. and Hernandez-Verdun, D. (1998). Presence of pre-rRNAs before activation of polymerase I transcription in the building process of nucleoli during early development of Xenopus laevis. *J. Cell Biol.* **142**, 1167-1180.
Wehner, K. A. and Baserga, S. J. (2002). The sigma(70)-like motif: a eukaryotic RNA binding domain unique to a superfamily of proteins required for ribosome biogenesis. *Mol. Cell* **9**, 329-339.

Table S1. Primer sequences (5′ to 3′)

Gene/construct	Forward	Reverse
Cloning		
Δ5′UTR PPan*	GTG*GCCTCTAGA***ATG**GGGAAAGATAAGACCAAGAAC	TCTAGATTACTTTCTCCTCTGCTTGAAGGG
PPanΔσ^{70}†	GAAGAGGGTCTTAGCGATGGCAAA	AGCGCTCTGCTGAGCCTTCATGTT
Full-length *c-Myc*	CTCGAGGGATTTATAAACGCGACCAAA	CTCGAGTTAGACAAAGTTCCTCAGCTG
RT-PCR		
5.8S rRNA	TCGCGACTCTTAGCGGTG	GGAGCGACCCTCAGACAG
PPan	TGTGCACAAGGTCACCCTAA	CCTCTCCGACTTCCTGTCTG
Pax6	TGCCCGACTCGACCAGACAGAAG	GCGCAGCACTCGGTTTATTGATGA
N-cam	GCCCCTCTTGTGGATCTTAGTGA	ACAGCGGCAGGAGTAGCAGTTC
GAPDH	GCCGTGTATGTGGAATCT	AAGTTGTCGTTGATGACCTTTGC
qRT-PCR‡		
PPan	AAACTCCTCCAGGAGAAA	CTTCACCAGCTGCAAAGTCATGCG

*Bold indicates the start codon; italics indicates mutations in the PPan MO1 binding site.
†Primers for inverse PCR were 5′-phosphorylated.
‡For detection of 5.8S rRNA and *GAPDH*, the same primers as for RT-PCR were used.